MJFAS MALAYSIAN JOURNAL OF FUNDAMENTAL AND APPLIED SCIENCES
PRINT ISSN: 2289-5981 | ONLINE ISSN: 2289-599X

RESEARCH ARTICLE

Nitric oxide removal by zinc chloride activated oil palm empty fruit bunch fibre

Cha Soon Lin[a], Naimah Ibrahim[a,*], Norhidayah Ahmad[a], Muhammad Adli Hanif[a], Sureena Abdullah[b]

[a] *Faculty of Civil Engineering Technology, Universiti Malaysia Perlis, Kompleks Pusat Pengajian Jejawi 3, 02600 Arau, Perlis, Malaysia*
[b] *Faculty of Chemical and Process Engineering Technology, Universiti Malaysia Pahang, Lebuhraya Tun Razak, 26300 Gambang, Kuantan, Pahang, Malaysia*

* *Corresponding author: naimah@unimap.edu.my*

Article history
Received 16 June 2020
Revised 8 October 2020
Accepted 22 October 2020

Graphical abstract

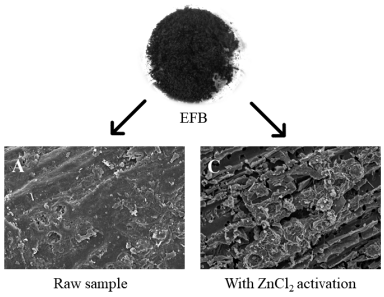

Abstract

Nitric oxide (NO) emission is known to pose detrimental effects towards the environment and human beings. Low-temperature NO removal by activated carbon from agricultural waste materials is affordable due to the use of low-cost materials as precursor and elimination of the need for flue gas reheating. The use of chemical agents in activated carbon production improves the performance of waste materials in NO removal. The performance of NO removal was investigated via breakthrough experiment using oil palm empty fruit bunch (EFB) activated with zinc chloride ($ZnCl_2$) at different concentrations (0.1, 0.5, and 1.5 M). Activation of EFB with 0.5 M $ZnCl_2$ resulted in the formation of well-defined micropores, but the use of higher concentration of $ZnCl_2$ resulted in widening of developed pores and intense pore blockage which reduce the accessibility of NO molecules to the adsorption sites. An adsorption isotherm study conducted using 0.5 M $ZnCl_2$/EFB sample with varying NO concentration between 300-1000 ppm indicated that the adsorption process was best defined by Langmuir isotherm model. In addition, adsorption kinetic was investigated at different temperatures; i.e. 100, 150, 200, 250 and 300 °C. NO removal was found to follow Avrami kinetic model at T=100 °C, while upon further increase in temperature, the process was better fitted to the pseudo-second order kinetic model. NO adsorption capacity increases significantly beyond 250 °C up to 1000 mg/g. The activation energy of NO adsorption fell into two distinct regions: -4.73 kJ/mol at 100-200 °C and 84.04 kJ/mol at 200-300 °C. At lower temperature, the adsorption process was exothermic and followed physisorption path, while the increase in reaction temperature led to slower rate of reaction. It was concluded that the removal of NO using EFB modified with $ZnCl_2$ at optimized condition could be a promising alternatives for treating NO-containing flue gas.

Keywords: Activated carbon, Industrial waste treatment, Nitric oxide adsorption, Oil palm empty fruit bunch, Waste conversion.

INTRODUCTION

Nitric oxide (NO) emissions are known to pose severe effects towards the environment e.g. photochemical smog, acid rain; and towards the human respiratory system. The major problems are typically minimized effectively by subjecting the NO gas through a post-treatment method such as selective catalytic reduction (SCR), selective non-catalytic reduction (SNCR), adsorption etc. The removal of NO via adsorption process is highly preferred due to the simplicity of the process, high removal percentage and low operational cost (Wu *et al.*, 2020).

Activated carbon is commonly utilized in adsorption processes as the precursor of these materials are easily found naturally or waste originated from other processes. In the palm oil milling process, 21-22% of empty fruit bunch (EFB) are generated for every tonne of fresh fruit bunch processed (Wafti *et al.*, 2017). As EFB is an agricultural waste with very low commercial value, the excessive amount discarded at palm oil mills may pose environmental problems. Using wastes produced in a process to treat pollution from other processes is deemed very attractive as multiple problems can be solved simultaneously. Several studies have reported utilizations of EFB as adsorbent in the context of gaseous pollutants adsorption. For instance, Meri *et. al.* (2018) compared the performance of hydrogel composite derived from EFB biochar and coal fly ash on H_2S adsorption, in which the former present longer breakthrough time and adsorption capacity. Studies by Joseph *et al.* (2017) and Kurniawan et al. (2019) indicated that EFB activated by CO_2 and KOH, respectively, was successful in adsorbing CO_2. EFB was also utilized in increasing the CO_2 capture of calcium oxide originated from the cockle shell (Mohamed *et al.*, 2019).

Carbonaceous materials can be activated via physical or chemical activation, with the latter being more widely preferred due to low utilization of activation energy and shorter activation time, while producing a high carbon yield. Dehydrating agents such as potassium hydroxide (KOH), phosphoric acid (H_3PO_4) and zinc chloride ($ZnCl_2$) are some examples of chemicals used for such purposes. Several studies have reported that the use of $ZnCl_2$ as the activating agent resulted in activated carbon with higher surface area and pore volume (Adhikari *et al.*, 2019; Cai *et al.*, 2019; Yagmur *et al.*, 2020).

In this study, the performance of NO removal by carbonaceous sorbent originated from oil palm empty fruit bunch chemically activated by $ZnCl_2$ was investigated. Different concentrations of $ZnCl_2$ were tested to obtain the ideal concentration of activating agent. The

isotherm and kinetic models of the adsorption process were evaluated by varying the inlet NO concentration and reaction temperature, respectively, and data were fitted to various models.

EXPERIMENTAL

Materials and chemicals

Fibres of oil palm EFB were collected from United Oil Palm Mill Sdn Bhd, Nibong Tebal, Pulau Pinang. The fibre was physically cleaned and oven dried at 110 °C for 24 hours to remove moisture. All the primary chemicals used were of analytical grade (AR). Zinc chloride was used without further purification.

Sample preparation and characterization

40 g of EFB was soaked in 200 mL of dehydrating agent, zinc chloride ($ZnCl_2$) at varying concentration (0.1, 0.5 and 1.5 M) for 12 hours at 110 °C. The EFB was then activated at 400 °C in a furnace for 2 hours. The activated sample was then washed with deionized water and rinsed to remove excess $ZnCl_2$ until the pH value of the sample reaches approximately 7. Then, the washed sample was oven dried at 110 °C for 24 hours. The prepared activated carbon was sieved to average particles sizes of 300 µm. The surface morphology of the raw and modified samples were characterized with Surface Electron Microscopy (SEM) on JEOL JSM-6460LA using SEI signal at magnification of 1,000 times. The Brunauer−Emmett−Teller (BET) specific surface area and pore characteristics was investigated using N_2 adsorption-desorption isotherm at 77 K on Micromeritics Tristar 3000. Surface area of the samples were calculated using BET equation while the pore characteristics were obtained via Barrett-Joyner-Halenda (BJH) method.

Adsorption experiment

The performance of modified EFB in removing NO was evaluated through a breakthrough experiment based on the study by Sumathi *et al.* (2014). This study was conducted using a horizontal quartz-column reactor (internal diameter=1.5 cm, length=25 cm) at 100 °C with 0.3 vol% NO/He (Linde). 2 g of the activated EFB was first flushed with He gas at 100 °C for 1 hour. Once stable reaction temperature was achieved, the gas flow was switched to simulated flue gas (1000 ppm NO, total flow rate=100 mL/min). The outlet NO concentration was constantly measured with a NO-NO_2 gas analyser until equilibrium was achieved. The adsorption capacity of the sorbent was calculated at equilibrium using Eq. (1) where Q_f, y_t, m_c, C_0 and C_A represent gas flow rate (L/min), gas molar fraction, mass of the adsorbent loaded in the column (g), the inlet concentration of the gas and gas concentration (mg/L) at breakthrough point, at C/C_o=0.05, respectively (Ahmad *et al.*, 2018):

$$q = \frac{C_0 Q_f y_t}{m_c} \int_0^{\infty} \left(1 - \frac{C_A}{C_0}\right) dt \quad (1)$$

Isotherm and kinetic studies

The study on adsorption isotherm was carried out using selected sorbent based on the performance of activated EFB in the previous breakthrough experiment with EFB modified by $ZnCl_2$ at different concentrations. The inlet concentration of NO was varied (300, 500, 700 and 1000 ppm) while the other reaction parameters mentioned earlier were maintained. The data obtained were fitted to four different isotherm models: Langmuir, Freundlich, Dubinin-Radushkevich and Temkin model.

Similarly, the kinetics of NO adsorption was studied using the same sorbent at five different temperatures (100, 150, 200, 250 and 300 °C). The experimental results were fitted with four kinetics models: pseudo-first order, pseudo-second order, Elovich and Avrami model. The activation energy of the reaction was calculated using the basic Arrhenius equation, given below:

$$\ln k = \frac{-E_a}{R}\left(\frac{1}{T}\right) + \ln A \quad (2)$$

where k is the rate constant, T is the temperature (K), A is the pre-exponential factor, E_a is the activation energy and R is the universal gas constant.

RESULTS AND DISCUSSION

Surface morphology

The SEM micrographs of raw and $ZnCl_2$ modified activated carbons are shown in Fig. 1. From Fig. 1(a), it can be seen that the surface of raw EFB activated carbon is relatively smooth and lacking of pores. The incorporation of 0.1 M of $ZnCl_2$ leads to the development of few micropores on the surface of EFB and upon further increase in $ZnCl_2$ concentration, more pores can be observed. This result is in agreement with the study by a previous work where insufficient utilization of $ZnCl_2$ was found to result in poor development of micropores on the surface of the sorbent (Shaaban *et al.*, 2015). An increment in $ZnCl_2$ concentration beyond 0.5 M however also results in widening of the pores as can be seen in Fig. 1(c). Additionally, excess amount of $ZnCl_2$ also leads to the blockage of the surface developed micropores which may not be removable during the washing and rinsing process (Liou & Wu, 2009) as seen in Fig. 1(d).

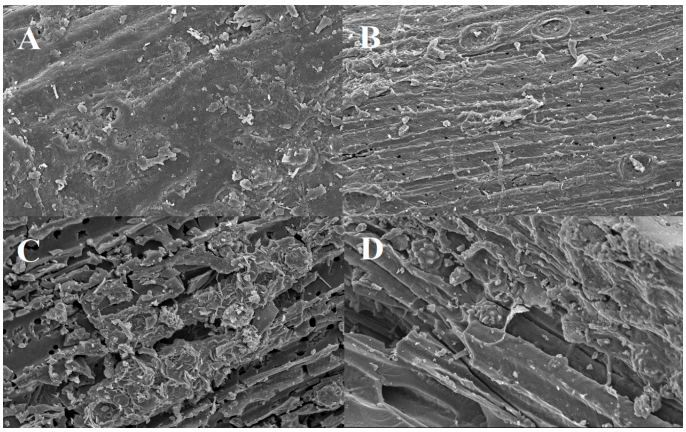

Fig. 1 SEM images of (a) raw EFB, (b) 0.1 M $ZnCl_2$/EFB, (c) 0.5 M $ZnCl_2$/EFB and (d) 1.5 M $ZnCl_2$/EFB at 1000x magnifications.

Surface area and pore analysis

The surface area and pore characteristics of all tested samples are summarized in Table 1. Raw EFB sample possess a very small available surface area and total pore volume. Upon modification with $ZnCl_2$, the surface area of the modified EFB increased with higher concentration of $ZnCl_2$ used, up to 0.5 M. Further increase in $ZnCl_2$ does not exhibit significant change as the surface area of 1.5 M $ZnCl_2$/EFB is similar to 0.5 M $ZnCl_2$/EFB. The total pore volume of the sorbents were significantly enhanced with the incorporation of $ZnCl_2$, however, these volumes are still considered very low. The average pore size of the sorbents was increased from 2.16 to 14.43 nm with the introduction of 1.5 M $ZnCl_2$. This supports the observation from SEM where the modification of EFB with high concentration of $ZnCl_2$ resulted in the widening of the pores. Based on the results, the porosity of the sorbents is a combination of micropores and mesopores.

Table 1 Surface area and pore characteristics of all samples.

Sample	Surface area (m^2/g)	Total pore volume (cm^3/g)	Average pore size (nm)
Raw	1.3	0.0002	2.16
0.1 M	16.2	0.0016	3.72
0.5 M	156.8	0.0021	5.79
1.5 M	155.5	0.0068	14.43

NO breakthrough analysis

The NO breakthrough curves of EFB activated by $ZnCl_2$ at different concentrations are shown in Fig. 2, while Table 2 summarizes the experimental results. It can be seen that introduction of $ZnCl_2$ on EFB results in minor improvement on NO adsorption capacity compared to raw EFB. The sorption bed of all samples achieved breakthrough within the first 35 seconds and became saturated after 1200-1800 seconds possibly because thin bed depth (small dosage) was used.

The NO adsorption capacity is slightly increased from raw EFB up to 0.5 M $ZnCl_2$/EFB and decreased upon further increase in $ZnCl_2$ concentration to 1.5 M. The enhancement of adsorption capacity upon the introduction of $ZnCl_2$ may be attributed to the increment of surface area and the generation of surface pores as can be seen from the results obtained via BET and SEM analysis. Greater surface area and developed pores provide additional sites for adsorbing NO. However, excess concentration of $ZnCl_2$ is detrimental towards the performance of the sorbent due to pore blockage caused by the excess $ZnCl_2$. These restricted the accessibility of NO adsorbate towards the active sites and subsequently reducing the adsorption capacity of the sorbent. Based on this result, 0.5 M $ZnCl_2$/EFB was used for isotherm and kinetic studies.

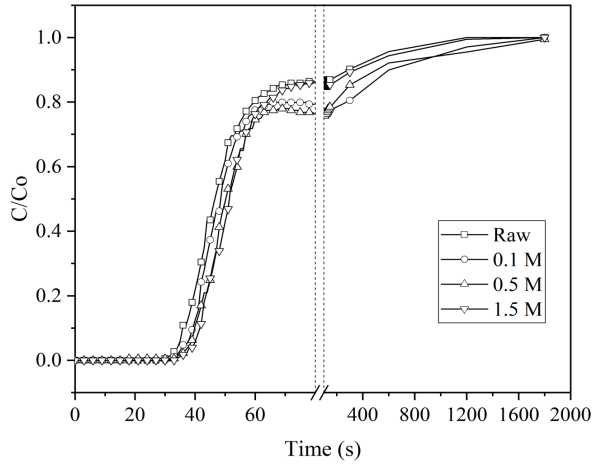

Fig. 2 Breakthrough curves of NO removal with raw and modified EFB

Table 2 Experimental results and NO adsorption capacity of all samples.

EFB sample	Break-through time (s) C/C_0=0.05	Time at C/C_0=0.5 (s)	Saturation time (s) C/C_0=0.99	Ads. capacity (mg/g)
Raw	29	46	1200	1.128
0.1 M	31	48	1800	1.423
0.5 M	20	50	1800	1.543
1.5 M	33	51	1800	1.378

Isotherm studies

Fig. 3 shows the breakthrough curves of NO adsorption by 0.5 M $ZnCl_2$/EFB sorbent using different inlet NO concentrations. In general, the performance of 0.5 M $ZnCl_2$/EFB sorbent in removing NO is highly affected by the inlet concentration of NO. Rising the inlet concentration typically results in the enhancement of NO sorption rate which can be ascribed to an increase in the driving force created by higher coverage of NO adsorbate at higher NO concentration. However, insufficient amount of sorbent at high NO concentration will lead to shorter breakthrough time due to fast saturation of the sorbent (Rosas *et al.*, 2012). In this study, the 0.5 M $ZnCl_2$/EFB sorbent can be seen to suffer from fast saturation as the highest NO removal was obtained at the lowest inlet NO concentration of 300 ppm. At an inlet concentration of 300 ppm, the sorption bed achieved a breakthrough around 75 seconds, which is 2 times longer compared to the other three higher NO concentrations. The NO adsorption capacity of the sorbent is in the order of: 300 ppm > 700 ppm > 1000 ppm > 500 ppm. The results of the breakthrough experiments using different NO inlet concentrations are summarized in Table 3.

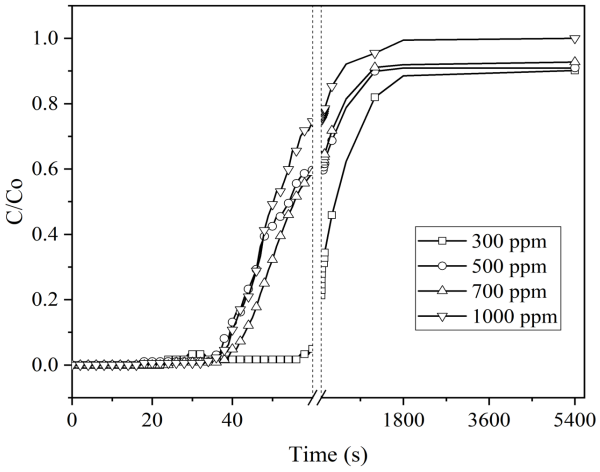

Fig. 3 Breakthrough curves of NO removal of 0.5 M $ZnCl_2$/EFB exposed to different inlet NO concentrations

Table 3 Experimental results of NO adsorption using different inlet concentration of NO.

NO inlet concentration (ppm)	Break-through time (s)	Equilibrium concentration (mg/L)	Adsorption capacity (mg/g)
300	75	40.18	2.23
500	36	66.70	1.18
700	39	93.75	1.67
1000	34	133.9	1.54

The experimental results were fitted to four different isotherm models: Langmuir, Freundlich, Dubinin-Radushkevich and Temkin model, with the Langmuir model demonstrating the best fit (R^2=0.90) to adsorption data. Similarly, the studies by Ammendola *et al.* (2017) and Tiwari *et al.* (2017) demonstrated that adsorption of CO_2 on activated carbons is best defined by the Langmuir model. This indicates that the adsorption of NO on $ZnCl_2$ activated EFB proceeds in a monolayer adsorption on the outer surface of the sorbent. Each NO adsorbate is adsorbed at a finite amount of well-defined localized sites, in which each site may hold only one NO adsorbate. During the adsorption process, the adsorption energies on the surface are considered to be uniform and no transmigration of NO adsorbate occurs (Edet & Ifelebuegu, 2020).The Langmuir isotherm fit is shown in Fig. 4, while the adsorption isotherm parameters of all tested models are summarized in Table 4.

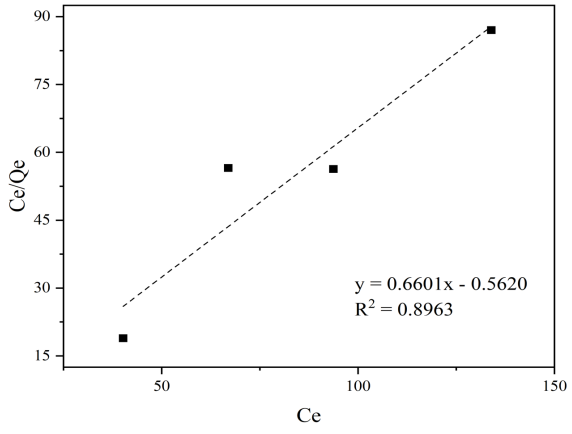

Fig. 4 Langmuir adsorption isotherm fit

Table 4 Adsorption isotherm parameters of all tested isotherm models

Model	Parameter	Unit	Values
Langmuir	K_L	atm^{-1}	1.35
	Q_s	mg/g	153.87
	R^2		0.90
	Δq	%	1.065
Freundlich	K_f	$mg/g.atm^{-1/n}$	314.14
	n		-6.28
	R^2		-9.08
	Δq	%	3.80
Dubinin-	K_{dr}	mg/g	-0.0095
Radushkevich	Q_{dr}		$8.04x10^{59}$
	R^2		-8.518
	Δq	%	4.2
Temkin	b_T		-101.98
	A_T		$6.69x10^{-5}$
	R^2		-0.774
	Δq	%	4.07

Kinetic studies

For kinetic studies, NO breakthrough tests were conducted at different temperatures of 100, 150, 200, 250 and 300 °C. The breakthrough curves and the corresponding data at different temperatures are shown in Fig. 5 and Table 5 respectively.

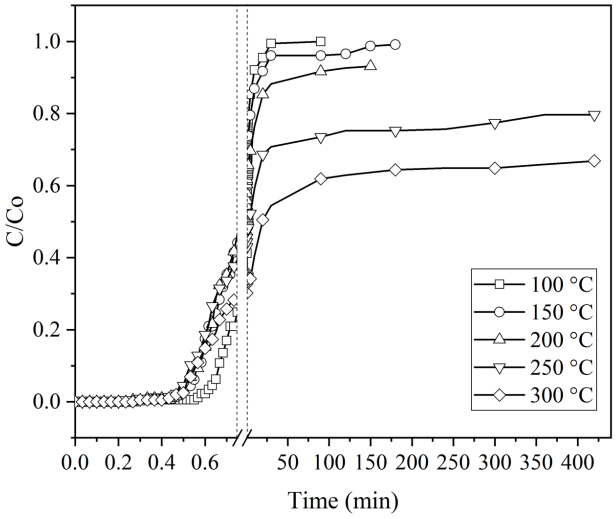

Fig. 5 Breakthrough curves of NO removal by 0.5 M $ZnCl_2$/EFB at different temperatures

Table 5 Experimental results of NO adsorption at different temperatures

T (°C)	Eq. time (s)	% NO removal at time (min)					Ads. Capacity (mg/g)
		20	90	180	300	420	
100	5400	0.41	-	-	-	-	154.2
150	10800	8.3	3.93	0.9	-	-	176.9
200	9000	14.7	8.3	-	-	-	183.2
250	25200	31.4	26.6	24.8	22.6	20.4	587.2[b]
300	25200	49.5	38.1	35.6	35.2	33.2	1105[c]

a,b,c – Adsorption capacity at C/C_0 = 0.93, 0.8 and 0.64, respectively

Based on the results, NO adsorption process can be said to be critically governed by the reaction temperature. As the reaction temperature increases, the sorbent took a longer time to achieve equilibrium and far from achieving saturation even after 7 hours. This phenomenon results in a significant improvement in NO adsorption capacity of the sorbent.

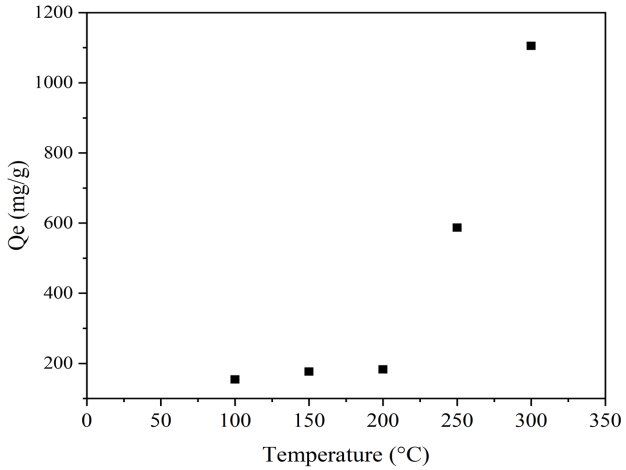

Fig. 6 NO adsorption capacity trend at different temperatures

The NO adsorption capacities obtained from the breakthrough study are plotted in Fig 6. The graph indicates the presence of two distinct temperature ranges of NO adsorption capacity: from 100-200 °C and from 200-300 °C. This can be explained by the transition or mixture of adsorption kinetics and mechanism influenced by the change in temperature. Hafeez *et al.* (2015) reported that NO adsorption does not exclusively follow intraparticle diffusion mechanism only, but may also involve other different adsorption mechanism at higher reaction temperature. Four kinetic models (pseudo-first order, pseudo-second order, Elovich, Avrami) were fitted with the experimental data to determine the possible adsorption mechanisms at different reaction temperatures. Table 6 shows complete adsorption kinetic parameters of all models.

Table 6 Adsorption kinetics parameters of all tested kinetic models

Model		Temperature (°C)				
		100	**150**	**200**	**250**	**300**
Pseudo 1st order	q_e, exp	154.2	176.9	183.2	587.1	1105
	K_1	0.778	0.054	0.051	0.006	0.005
	R^2	0.767	0.659	0.596	0.354	0.483
	q_e, cal	74.14	55.38	64.33	434.0	897.9
	Δq	4.2	5.48	5.19	2.07	1.49
Pseudo 2nd order	q_e, exp	154.2	176.9	183.2	587.1	1105
	K_2	0.004	0.004	0.003	$2x10^{-4}$	$7.4x10^{-5}$
	R^2	0.173	**0.969**	**0.967**	**0.963**	**0.900**
	q_e, cal	160.9	183.9	173.2	532.8	961.3
	Δq	0.355	0.314	0.44	0.73	1.03
Elovich	q_e, exp	154.2	176.9	183.2	587.2	1105
	b	0.022	0.029	0.026	0.014	0.008
	a	477.5	640.7	550.0	536.9	625.6
	R^2	0.835	0.713	0.75	0.817	0.827
	q_e, cal	240	310	290	560	910
	Δq	4.5	6	4.67	0.36	1.4

Avrami	$q_{e,exp}$	154.2	176.9	183.2	587.2	1105
	n	1.59	1.102	1.146	0.894	0.969
	K_{av}	1.014	0.678	0.664	0.133	0.095
	R^2	**0.948**	0.799	0.730	0.705	0.727
	$q_{e,cal}$	158.5	197.8	201.5	608.0	996.7
	Δq	0.226	0.84	0.80	0.28	0.78

A comparison of R^2 values (near to 1) and Δq (%) (smaller) at all reaction temperature from Table 6 reveals that pseudo-second order kinetic model gives best fit for all temperature except for 100 °C, where the reaction at such temperature is better defined by the fractional order Avrami kinetic model. This result suggests that NO adsorption on $ZnCl_2$ modified EFB is a multi-linear process with multiple adsorption pathways (Songolzadeh *et al.*, 2015).

At higher temperature, the adsorption is proportional to the number of free available sites on the surface of the adsorbent (Singh & Kumar, 2016). The decreasing second order rate constant of the pseudo-second order model from 150 to 300 °C indicates that NO adsorption is an exothermic reaction (Tiwari *et al.*, 2017). The adsorption data fitted to Avrami and pseudo-second order model are shown in Figs. 7 and 8 respectively.

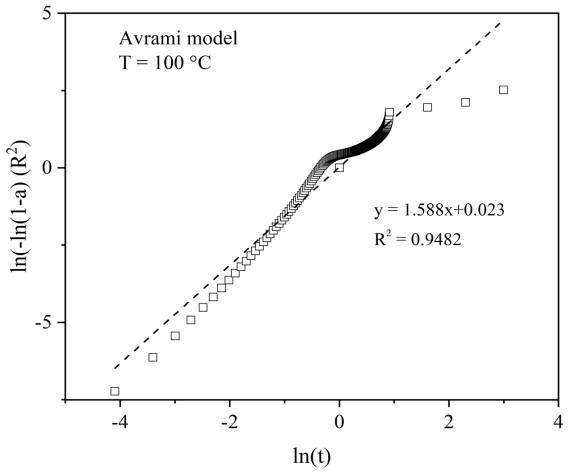

Fig. 7 Avrami adsorption model fit at 100 °C

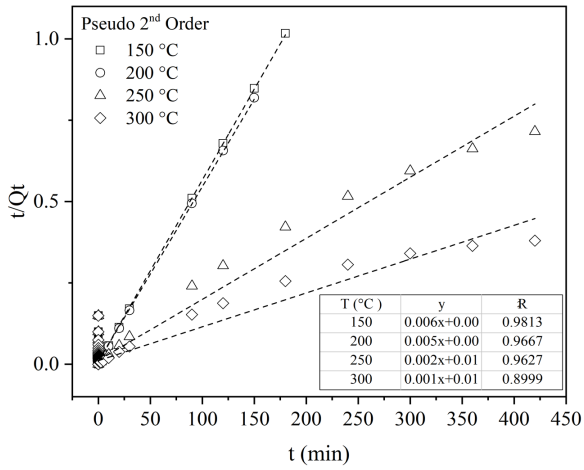

Fig. 8 Pseudo second order adsorption model fit at 150-300 °C

Activation energy

All Arhenius parameters are summarized in Table 7, while the Arrhenius plot is shown in Fig. 9. Similar to adsorption capacity, the activation energy of NO adsorption shows two different regimes at low temperature range of 100-200 °C and higher temperature between 200-300 °C. In the lower temperature range, the activation energy for NO adsorption is calculated to be -4.73 kJ/mol. Upon further increase in temperature, the activation energy of the process becomes more exothermic at -84.04 kJ/mol. A negative activation energy at all temperature indicates that NO adsorption is an exothermic reaction and the NO molecules were adsorbed via physisorption (Goel *et al.*, 2015). The result also indicates that the rate of reaction decreases at higher reaction temperature (Tiwari *et al.*, 2017). This is proven in previous kinetic studies where the sorption at 100 °C ends after 90 minutes while at 300 °C, the reaction is far from completed even after 7 hours.

Table 7 Arrhenius equation parameters at different temperature range

Temperature (°C)	Parameters	Values
100-200	Ea	-4.73
	A	0.056
200-300	Ea	-84.04
	A	8.08×10^{-11}

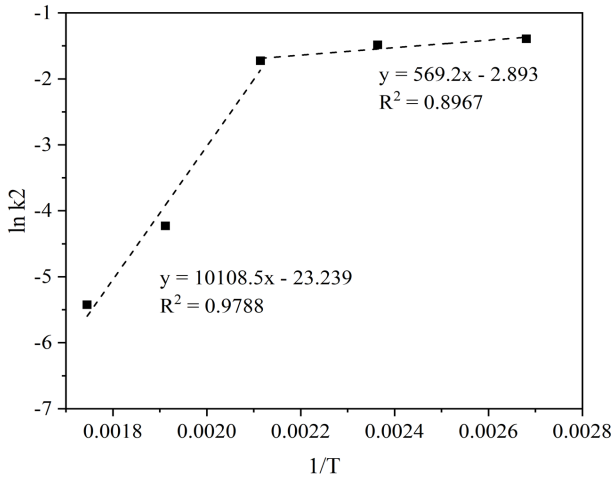

Fig. 9 Arrhenius equation plot

In a physisorption process, the increase in reaction temperature reduces the intermolecular forces between the NO adsorbate and EFB sorbent which possibly hinders the adsorption process to take place (Singh & Kumar, 2016). The weak interaction between adsorbate and adsorbent may also lead to desorption of adsorbed NO molecules at higher temperature. The Arrhenius pre-exponential factor, A, also significantly decreases from 0.055 to 8.08×10^{-11} upon the increase in temperature beyond 200 °C. The reduction in the value of A signifies that the fractions of NO molecules with energy higher or equal to activation energy decreased substantially, resulting in lower successful collision between NO molecules and EFB (Kudahi *et al.*, 2017).

CONCLUSION

In this study, the influence of $ZnCl_2$ activation on empty fruit bunch on the removal of toxic NO gas was investigated. The optimal concentration of $ZnCl_2$ was found to be 0.5 M as it promotes formation of micropores on the surface of the sorbent. Excess $ZnCl_2$ was detrimental towards NO removal due to pore blockage which hindered NO molecules from accessing the adsorption sites as well as pore widening. NO adsorption on EFB demonstrated higher adsorption capacity at lower inlet NO concentration and the process was best fitted to Langmuir isotherm. The kinetic study indicates that the increase in temperature can lead to transition or mixture of adsorption kinetics and mechanism. The sorption process followed Avrami model at 100 °C, but was better defined by the pseudo-second order model at higher temperature. The activation energy of NO adsorption was in the range of -4.73 to -84.04 kJ/mol depending on the reaction temperature range. The NO adsorption was an exothermic process and the adsorbates were

mainly adsorbed via physisorption. The increase of reaction temperature led to slower rate of reaction, but resulted in higher NO adsorption capacity. The adsorption capacity of EFB may be improved by treating the EFB with acid or additives before adding $ZnCl_2$ which will result in the formation of oxygen functional groups. The sorbent may also be subjected to thermal activation which will increase the surface area and porosity of the sorbent.

ACKNOWLEDGEMENT

The authors would like to acknowledge the support from the Fundamental Research Grant Scheme (FRGS) under a grant number of FRGS/2/2013/SG01/UNIMAP/02/1 from the Ministry of Higher Education Malaysia.

REFERENCES

Adhikari, S., Pokharel, B., Gurung, V., Shrestha, R. M., Rajbhandari, R. 2019. Preparation and Characterization of Activated Carbon from Walnut (Jaglansregia) Shells by Chemical Activation with Zinc Chloride ($ZnCl_2$). *Proceedings of IOE Graduate Conference, 2019-Winter* 7, 15–20. https://doi.org/10.3923/jas.2012.1124.1129

Ahmad, N., Yong, S. H., Ibrahim, N., Md Ali, U. F., Muhammad Ridwan, F., Ahmad, R. 2018. Optimisation of Copper Oxide Impregnation on Carbonised Oil Palm Empty Fruit Bunch for Nitric Oxide Removal using Response Surface Methodology. *E3S Web of Conferences* 34, 02029. https://doi.org/10.1051/e3sconf/20183402029

Ammendola, P., Raganati, F., Chirone, R. 2017. CO_2 adsorption on a fine activated carbon in a sound assisted fluidized bed: Thermodynamics and kinetics. *Chem. Eng. J.* 322, 302–313. https://doi.org/10.1016/j.cej.2017.04.037

Cai, Y., Liu, L., Tian, H., Yang, Z., Luo, X. 2019. Adsorption and Desorption Performance and Mechanism of Tetracycline Hydrochloride by Activated Carbon-Based Adsorbents Derived from Sugar Cane Bagasse Activated with $ZnCl_2$. *Molecules* 24, 4534.

Edet, U. A., Ifelebuegu, A. O. 2020. Kinetics, isotherms, and thermodynamic modeling of the adsorption of phosphates from model wastewater using recycled brick waste. *Processes* 8, 665. https://doi.org/10.3390/PR8060665

Goel, C., Bhunia, H., Bajpai, P. K. 2015. Resorcinol-formaldehyde based nanostructured carbons for CO_2 adsorption: Kinetics, isotherm and thermodynamic studies. *RSC Adv.* 5, 93563–93578. https://doi.org/10.1039/c5ra16255f

Hafeez, S., Fan, X., Hussain, A., Martín, C. F. 2015. CO_2 adsorption using TiO_2 composite polymeric membranes: A kinetic study. *J. Environ. Sci.* 35, 163–171. https://doi.org/10.1016/j.jes.2015.04.019

Joseph, C. G., Quek, K. S., Daud, W. M. A. W., Moh, P. Y. 2017. Physical Activation of Oil Palm Empty Fruit Bunch via CO_2 Activation Gas for CO_2 Adsorption. *IOP Conf. Ser. Mater. Sci. Eng.* 206, 012003. https://doi.org/10.1088/1757-899X/206/1/012003

Kudahi, S. N., Noorpoor, A. R., Mahmoodi, N. M. 2017. Determination and analysis of CO_2 capture kinetics and mechanisms on the novel graphene-based adsorbents. *J. CO_2 Util.* 21, 17–29. https://doi.org/10.1016/j.jcou.2017.06.010

Kurniawan, I. D. O., Kurniawan, R. Y., Widiastuti, N., Atmaja, L., Shofiyani, A. 2019. Development of Activated Carbon Material from Oil Palm Empty Fruit Bunch for CO_2 Adsorption. *J. Tek. ITs* 8(2), F86–F94.

Liou, T.-H., Wu, S.-J. 2009. Characteristics of microporous/mesoporous carbons prepared from rice husk under base- and acid-treated conditions. *J. Hazard. Mater.* 171, 693–703. https://doi.org/10.1016/j.jhazmat.2009.06.056

Meri, N. H., Alias, A. B., Talib, N., Rashid, Z. A., Ghani, W. A. W. A. K. 2018. Comparison of H_2S adsorption by two hydrogel composite (HBC) derived by Empty Fruit Bunch (EFB) biochar and Coal Fly Ash (CFA). *IOP Conf. Series: Mater. Sci. Eng.* 334, 012038. https://doi.org/10.1088/1757-899X/334/1/012038

Mohamed, M., Yusup, S., Loy, A. C. M. 2019. Effect of Empty Fruit Bunch in Calcium Oxide for Cyclic CO_2 Capture. *Chem. Eng. Technol.* 42(9), 1840–1851. https://doi.org/10.1002/ceat.201800649

Rosas, J. M., Ruiz-Rosas, R., Rodríguez-Mirasol, J., Cordero, T. 2012. Kinetic study of NO reduction on carbon-supported chromium catalysts. *Catal. Today* 187, 201–211. https://doi.org/10.1016/j.cattod.2011.10.032

Shaaban, A., Se, S. M., Ibrahim, I. M., Ahsan, Q. 2015. Preparation of rubber wood sawdust-based activated carbon and its use as a filler of polyurethane matrix composites for microwave absorption. *New Carbon Mater.* 30(2), 167–175. https://doi.org/10.1016/S1872-5805(15)60182-2

Singh, V. K., Kumar, E. A. 2016. Comparative Studies on CO_2 Adsorption Kinetics by Solid Adsorbents. *Energy Procedia* 90, 316–325. https://doi.org/10.1016/j.egypro.2016.11.199

Songolzadeh, M., Soleimani, M., Takht Ravanchi, M. 2015. Using modified Avrami kinetic and two component isotherm equation for modeling of CO_2/N_2 adsorption over a 13X zeolite bed. *J. Nat. Gas Sci. Eng.* 27, 831–841. https://doi.org/10.1016/j.jngse.2015.09.029

Sumathi, S., Bhatia, S., Lee, K. T., Mohamed, A. R. 2014. Sorption of SO_2 and NO by modified palm shell activated carbon: Breakthrough curve model. *Pertanika J. Sci. Technol.* 22(1), 307–314.

Tiwari, D., Goel, C., Bhunia, H., Bajpai, P. K. 2017. Dynamic CO_2 capture by carbon adsorbents: Kinetics, isotherm and thermodynamic studies. *Sep. Purif. Technol.* 181, 107–122. https://doi.org/10.1016/j.seppur.2017.03.014

Wafti, N. S. A., Lau, H. L. N., Loh, S. K., Aziz, A. A., Rahman, Z. A., May, C. Y. 2017. Activated carbon from oil palm biomass as potential adsorbent for palm oil mill effluent treatment. *J. Oil Palm Res.* 29(2), 278–290. https://doi.org/10.21894/jopr.2017.2902.12

Wu, R., Ye, Q., Wu, K., Cheng, S., Kang, T., Dai, H. 2020. Adsorption performance of CMK-3 and C-FDU-15 in NO removal at low temperature. *J. Environ. Sci.* 87, 289–298. https://doi.org/10.1016/j.jes.2019.07.014

Yagmur, E., Gokce, Y., Tekin, S., Semerci, N. I., Aktas, Z. 2020. Characteristics and comparison of activated carbons prepared from oleaster (Elaeagnus angustifolia L.) fruit using KOH and $ZnCl_2$. *Fuel* 267, 117232. https://doi.org/10.1016/j.fuel.2020.117232